J-Researchers

Journal of Civil Engineering Researchers

Journal homepage: www.journals-researchers.com

# Numerical Analysis of the Steel Fiber Reinforced Concrete Piles And Prestressed Concrete Beam

Fatiha. Iguetoulene[a,*] Youcef. Bouafia[a] Said. Kachi[a]

[a] University Mouloud Mammeri of Tizi-Ouzou , Civil Engineering, 15000 Algeria

**ABSTRACT**

This paper studies the structural behavior of prestressed concrete beams and steel fiber reinforced concrete piles. A nonlinear finite element formulation based on the principle of virtual work is developed to analyze the response of these prestressed structural elements under applied loads. The model accounts for material nonlinearity, second-order effects, and variable stiffness through an incremental loading procedure. Simpson's integration scheme is adopted to evaluate the cross-sectional response of each element. The governing equations describing beam behavior are established, and the influence of compressive strength and prestressing force on structural performance is examined. Experimental tests conducted on prestressed concrete beams and steel fiber–reinforced concrete piles are used to validate the proposed approach. A comparison between numerical and experimental results demonstrates the accuracy and reliability of the developed formulation.

**ARTICLE INFO**

Received: January 09, 2026
Accepted: February 20, 2026

***Keywords:***
*Prestressed concrete beams*
*Steel fiber-reinforced concrete*
*Piles*
*Nonlinear finite element analysis*
*Virtual work principle*
*Constitutive modeling*
*Experimental validation*



DOI: 10.61186/JCER.8.1.1
DOR: 20.1001.1.22516530.1399.11.4.1.1

## 1. Introduction

The modeling and nonlinear analysis of reinforced and fiber-reinforced concrete structures require accurate formulations of the nonlinear system of equations, as discussed by Bouafia et al. (2002), Seung–Eock Kim et al. (2001), Sun and Chan (2017), and Grelat and Iguetoulene (2017) [1–2,5,7]. These studies emphasize the importance of considering both the global structural response and the local behavior each element simultaneously. Significant research efforts have been devoted to improving nonlinear analysis procedures, particularly in the formulation of the tangent stiffness matrix. Methods proposed by Riks (1972), Albermani et al. (2004), and Park S.H. et al. (2012) [2–3,10] have contributed substantially to this field. However, these approaches may fail to capture high-frequency modes accurately and can result in non-symmetric tangent stiffness matrices.Various models of fiber-reinforced concrete have been integrated into previous studies to improve the representation of post-cracking and ductile behavior (e.g., Bazeos and Xykis, 2002; Park S.H. et al., 2012) [11–12].

In this paper, a numerical formulation based on the principle of virtual work is presented to model and analyze the nonlinear structural response under external loading [12,19]. The governing equilibrium equations are derived, and the solution procedure for these equations is discussed. Constitutive laws for both conventional concrete and fiber-

* correspondence E-mail: iguetouene_fatiha@yahoo.fr

reinforced concrete are then introduced, followed by a description of the structural equilibrium formulation. Fiber-reinforced concrete is increasingly used in modern structures due to its enhanced mechanical properties and durability compared to conventional concrete. The addition of fibers synthetic, steel, or natural improves tensile strength, crack resistance, and impact performance, which are critical for structural elements subjected to complex loading conditions (Jamshidi, 2023; Parvinnejad et al., 2022; Kameli, Shahi & Mahboob, 2024) [20–22]. Recent studies have employed numerical modeling to better understand and predict the behavior of FRC. For instance, Zedan and Khan (2023) developed a model to predict optimal mechanical properties based on fiber type and proportion, while Al Mahaidi et al. (2022) [23–24] applied the finite element method to analyze reinforced concrete beams strengthened with FRP composites. These studies demonstrate that fiber integration and advanced numerical modeling are complementary approaches for improving structural safety and efficiency. Nevertheless, systematic comparisons between experimental and numerical results remain essential to validate models and ensure their applicability in practical engineering contexts.

In this study, a numerical formulation based on the principle of virtual work is presented to model and analyze the nonlinear behavior of prestressed concrete beams and reinforced concrete truss beams under external loads. The analysis accounts for the actual behavior of concrete and steel, including cracking, steel yielding, and failure mechanisms. A nonlinear calculation program developed in Fortran was validated through comparison with experimental results.

## 2. Material and methods

### *2.1 BEHAVIOR OF BOTH MATERIALS*

**Compression and traction**

The material in compression the law of Sargin [7] is used, the tensile behavior will be modeled by the law of Grelat [7]

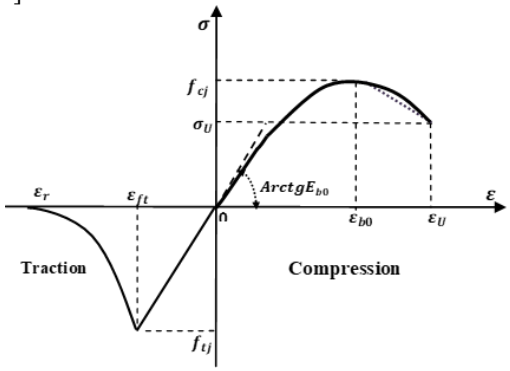


Figure 1. constitutive law of the concrete

The laws in compression and in traction are given in figure 1; and the Stress – Strain of reinforced fiber concrete Bouafia and al. [1] is given in figure2

$$\boldsymbol{\sigma} = f_{cj}\,\frac{k_b.\bar{\varepsilon}+(k_b'-1)\bar{\varepsilon}^2}{1+(k_b-2)\bar{\varepsilon}+k_b'\bar{\varepsilon}^2} \qquad (1)$$

With

$$\bar{\varepsilon} = \frac{\varepsilon}{\varepsilon_{b0}},\ k_b = \frac{E_{b0}\,.\varepsilon_{b0}}{f_{cj}}$$

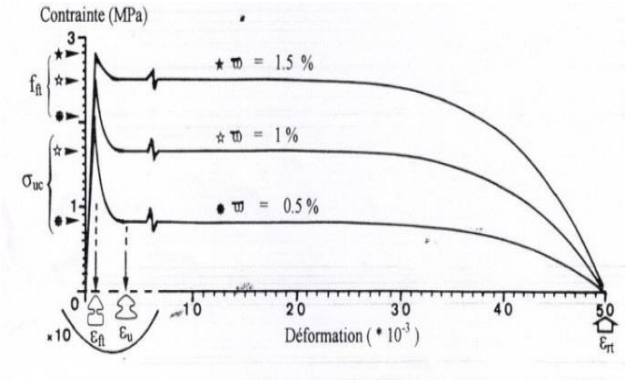


Figure 2. Stress – Strain of steel fiber concrete Bouafia and al. [1]

$$\begin{cases} \sigma = E_{ct}\varepsilon & si \quad 0 \le \varepsilon \le \varepsilon_u \\ \sigma = \sigma_{uc} - [\sigma_{uc} - f_{ft}]\dfrac{(\varepsilon-\varepsilon_u)^6}{(\varepsilon_{ft}-\varepsilon_u)^6} & si \quad \varepsilon_{ft} \le \varepsilon \le \varepsilon_u \\ \sigma = \sigma_{uc}\left[1 - \dfrac{(\varepsilon-\varepsilon_u)^6}{(\varepsilon_r-\varepsilon_u)^6}\right] & si \quad \varepsilon_u \le \varepsilon \le \varepsilon_r \end{cases} \qquad (2)$$

### *2.2 Section Equilibrium*

The section is discretized into a series of segments, Each part of the structure is discretized into beam elements. The Geometric description of the cross-section is given by:

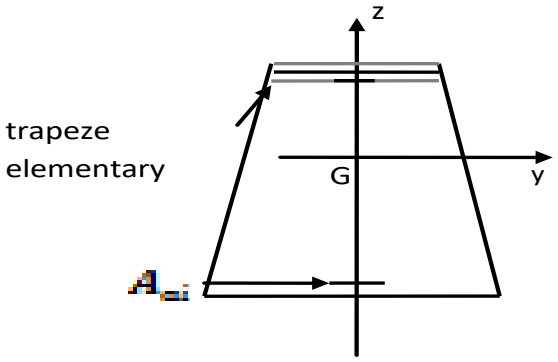


Figure 3. Discretization of the section into trapezoidal segments

The element calculation is using the given following relation:

$$\begin{pmatrix}\Delta F_{sn}\\ \Delta F_{st}\end{pmatrix} = [K_s].\begin{pmatrix}\Delta\varepsilon_n\\ \Delta\varepsilon_t\end{pmatrix} \quad (3)$$

where $\Delta \boldsymbol{F}_{sn}$ and $\Delta \boldsymbol{F}_{st}$ are normal forces increase and shear forces increasing .

$\Delta\varepsilon_n$ $\Delta\varepsilon_t$ the normal and tangential strains increase

$[\boldsymbol{K}_s]$: cord sections stiffness matrix

$$[\boldsymbol{K}_s] = \begin{bmatrix}[\boldsymbol{K}_{mn}]+[\boldsymbol{K}_{fn}] & [\boldsymbol{K}_{fnt}]\\ {}^t[\boldsymbol{K}_{fnt}] & [\boldsymbol{K}_{mt}]+[\boldsymbol{K}_{ft}]\end{bmatrix} \quad (4)$$

where $[\boldsymbol{K}_{mn}]$ is cord stiffness matrix linked the increase of the normal forces and the sections normal strains increase.

$$= \int E_m(y,z)\cdot\begin{bmatrix}1 & z & y\\ z & z^2 & yz\\ y & yz & y^2\end{bmatrix}\cdot dS_m \quad (5)$$

$[\boldsymbol{K}_{mt}]$ :cord stiffness matrix given by:

$$[\boldsymbol{K}_{mt}] = \begin{bmatrix}G\cdot A_y & 0 & 0\\ 0 & G\cdot A_z & 0\\ 0 & 0 & G\cdot I_x\end{bmatrix} \quad (6)$$

$$[\boldsymbol{K}_{fnt}] = \sum_{i=1}^{n_f} E_{fi}\cdot s_{fi}\cdot\sin\alpha i\cdot\cos^2\alpha i\cdot\begin{bmatrix}\cos\beta i & \sin\beta i & y_{fi}\sin\beta i - z_{fi}\cos\beta i\\ z_{fi}\cos\beta i & z_{fi}\sin\beta i & z_{fi}\cdot y_{fi}\sin\beta i - z_{fi}^2\cos\beta i\\ y_{fi}\cos\beta i & y_{fi}\sin\beta i & y_{fi}^2\sin\beta i - y_{fi}\cdot z_{fi}\cos\beta i\end{bmatrix}, \quad (7)$$

$$[\boldsymbol{K}_{ftm}] = [\boldsymbol{K}_{fmt}]^t \quad (8)$$

$$[\boldsymbol{K}_{ft}] = \sum_{i=1}^{n_f} E_{fi}\cdot\sin^2\alpha i\cdot s_{fi}\cdot V_{fti}\cdot {}^tV_{fti} \quad (9)$$

$$V_{fti} = \begin{pmatrix}\cos\beta_i\\ \sin B_i\\ y_{fi}\sin\beta_i - z_{fi}\cos\beta_i\end{pmatrix}. \quad (10)$$

The equilibrium of the section is determined by evaluating the determinant of the section stiffness matrix [Ks] and verifying the reinforcement failure criteria. If these conditions are met, the system of equations is solved.

$$\{\Delta F_s\} = [K_s].[\Delta\varepsilon_s] \quad (11)$$

Then, a convergence test is performed.

*2. 3 Calculation Steps*

The flowchart presents the numerical procedure used to analyze the structural behavior. The load is applied incrementally, and the stiffness matrix is updated at each step. For each element, section integration is performed and internal forces are computed. The equilibrium equations are then solved iteratively until convergence between internal and external forces is achieved. The process continues until the final load level is reached.

## 3 .Results and Discussions

*3.1 FOURE test*

This study is based on a series of tests performed by Foure [1] (OG1, OG2, OG3, OG4, ...).

Among these, the OG3 beam was analyzed. It is a simply supported beam with a span of 3 m between supports and a spacing of 0.5 m between the applied loads. The experimental setup and procedure are described in detail in Ref. [6]. The mechanical properties measured from material samples are presented in Tables 1 and 2.

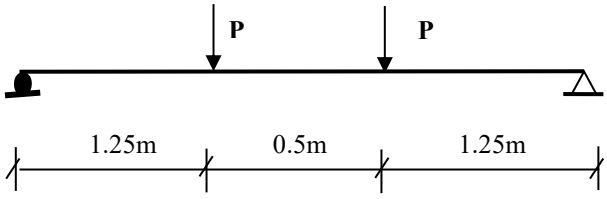


Figure 4. OG3 beam

Table 1.
Mechanical characteristics of the sample

| Reference | Diameter $\phi$(mm) | Module $E_a$(MPa) | Elasticity limit $f_e$(MPa) | Stress of rupture $f_r$ |
|---|---|---|---|---|
| OG3 | 16 | $2.05\times10^5$ | 575 | 700 |
| | 6 | $2.05\times10^5$ | 215 | 700 |

Table 2.
Mechanical properties of concrete obtained from specimen testing

| Mixed | Age $j$ (day) | Compression | | | | Traction (Bending) |
|---|---|---|---|---|---|---|
| | | $f_{cj}$ (Mpa) | $E_{ij}$ (MPa) | $E_d$ (MPa) | $\varepsilon_b$(‰) | $f_{tj}$ (MPa) |
| OG3 | 44 | 51.3 | 41600 | 42750 | 1.58 | 2.8 |

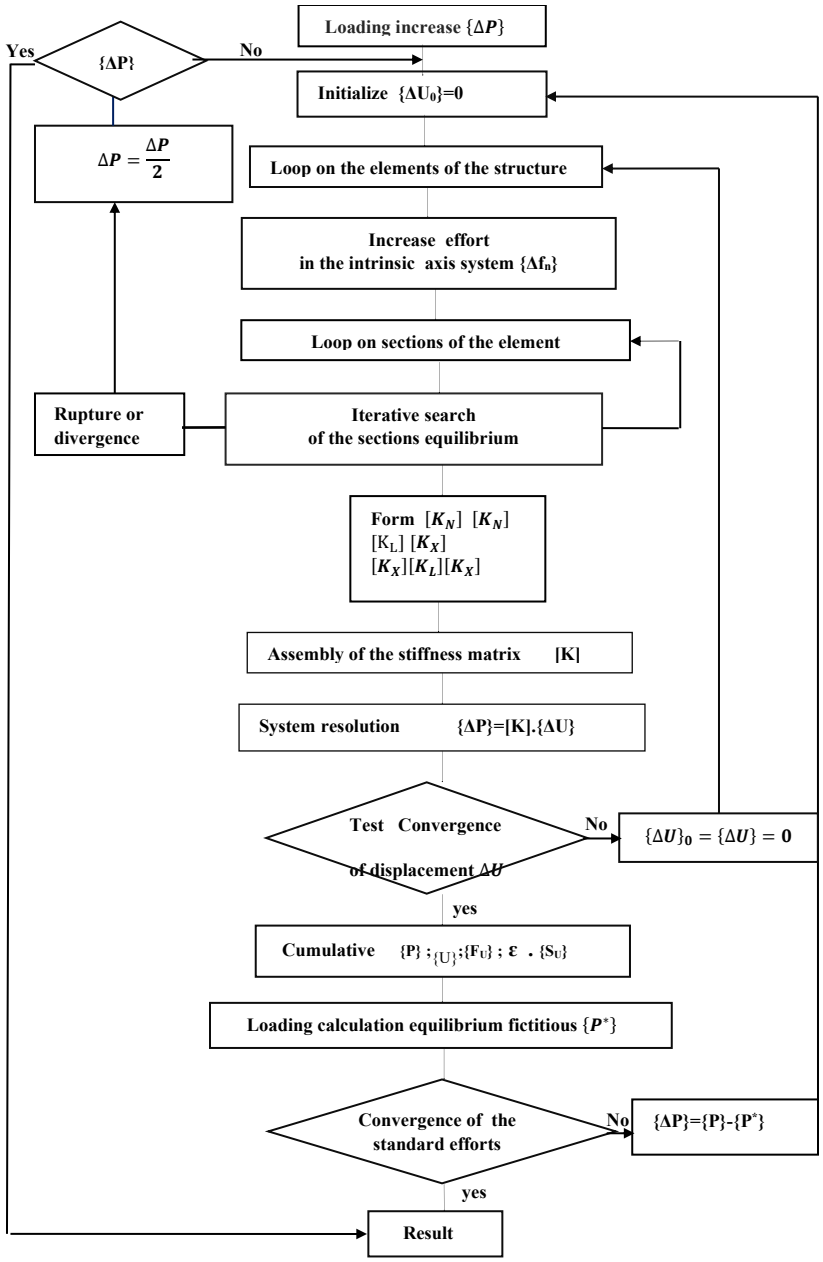


Figure 5. Flowchart of the Calculation Process

As can be seen in Figure 6, there is good agreement between the calculated and experimental results. The calculated failure load is 75.89 kN, while the experimental failure load is 78.04 kN.

As can be seen in Figure 6, there is good agreement between the calculated and experimental results. The calculated failure load is 75.89 kN, while the experimental failure load is 78.04

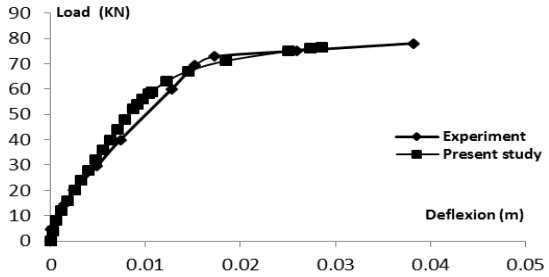


Figure 6. Load–deflection curve for beam OG3

### 3.2 Contiinous beam : Test conducted by BOUAFIA (OH4) [04]

The continuous beam test (OH4) was conducted at CEBTP by Y. Bouafia [04]. The beam features a double T-shaped cross-section, rests on two simple supports spaced 3.75 m apart, and is extended by a 1.25 m cantilever.

The laboratory experiment is described in detail in Ref. [04]. The mechanical characteristics measured on the samples are presented in tables 3.

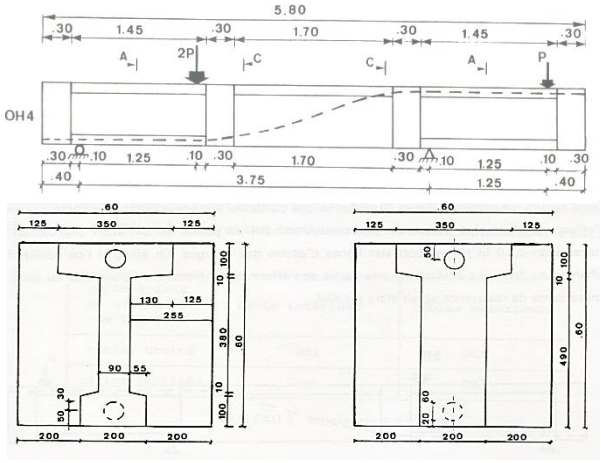


Figure 7. Construction details of the beam

Table 3.
Mechanical characteristics of concrete (Bouafia [04]).

| Reference | Age day | Module $E_{b0}$ (Mpa) | Stress $f_{cj}$ (MPa) | $\varepsilon_{b0}$(‰) | $f_{tj}$ (Mpa) |
|---|---|---|---|---|---|
| OH4 | 37 | 32070 | 34,50 | 0 ,16 | 3,30 |

The passive reinforcement of beam OH4 is made of cold-worked steel with a diameter of 5 mm. Prestressing is applied by post-tensioning. The cable is composed of 6 strands of Ø13 mm and is placed inside a flexible jacket. The initial prestressing force at the anchorage is 556 kN.

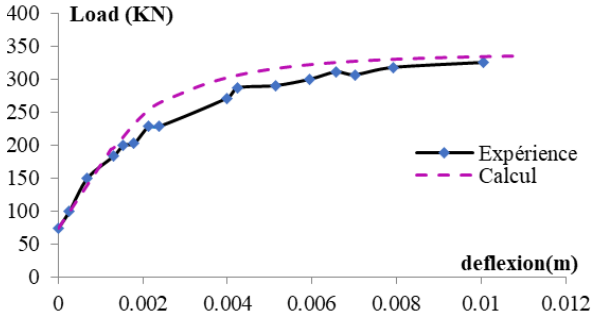


Figure 8. Load-deflexion curve for the beam OH4

The numerical curve closely matches the experimental curve, indicating that the modeling accurately predicts the structural behavior.

### 3.3 Bending composite on the pile

The experimental tests were conducted by Zhan [13] at the CEBTP laboratory. The piles, 500 mm in diameter, were made of control concrete, reinforced concrete, and fiber-reinforced concrete. The reinforcement of the reinforced concrete piles consists of five HA steel bars with a diameter of 16 mm (0.5 % by volume) in the scale test.

The piles were subjected to combined bending, with a normal compressive force of 1370 kN applied using external prestressing. The geometric characteristics of the piles are shown in Figure 10.

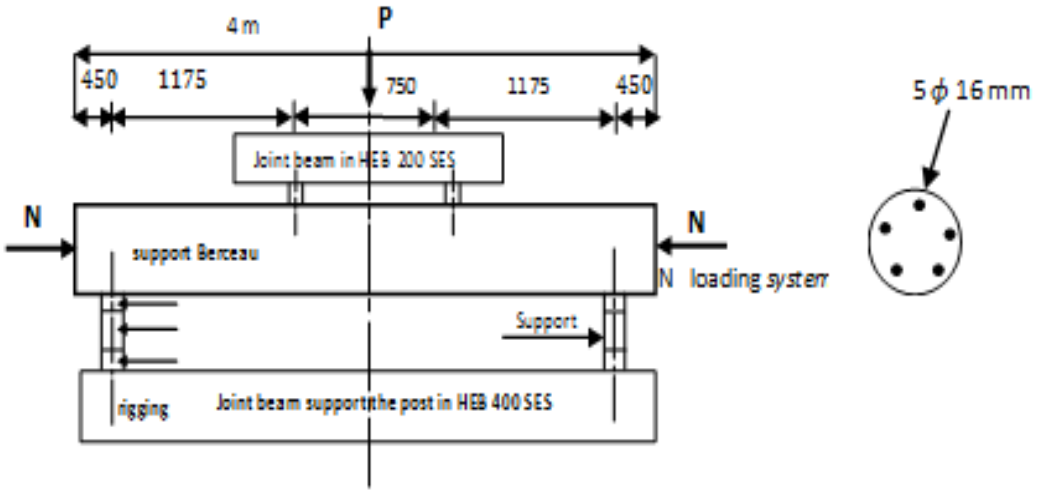


Figure 9. Combined bending test on a reinforced concrete pile with a circular cross-section

Table 4.
Mechanical properties of the composite (reinforced concrete with steel fibers) measured on cylinders (Zhan [13]).

| Indexof the test piece | $f_{cj}$ (MPa) | $f_{tj}$ (MPa) | $E_{b0}$ (GPa) | $R_b$ | $R_c$ | $\varepsilon_{rt}$ (‰) | $\varepsilon_0$ (‰) | $\varepsilon_{cu}$ (‰) |
|---|---|---|---|---|---|---|---|---|
| BFAC | 47.6 | 3.37 | 38.18 | 1.6 | 0.7 | –50 | 2.1 | 3.5 |

| Indexof the test piece | $E_a$ (GPa) | $l_f$ (mm) | $\omega$(%) | $\phi$ (mm) | $\varepsilon_u$ (‰) | $\tau_u$ (Mpa) |
|---|---|---|---|---|---|---|
| BFAC | 200 | 60 | 0.31 | 1 | –0.74 | 7 |

BFAC: Steel Fiber Reinforced Concrete.

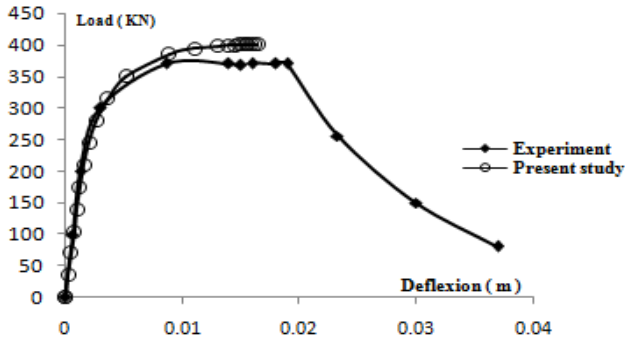


Figure 10. Comparison of calculated results with experimental results for a BFAC pile

For the reinforced concrete pile with steel fibers at 25 kg/m³ (BFAC), the experimentally measured ultimate load is 390 kN, while the numerical prediction is 400.15 kN.

In both the linear and nonlinear phases corresponding to crack initiation and propagation with the contribution of the concrete fibers the numerical results show good agreement with the experimental data.

In the post cracking phase, where the fiber-reinforced concrete contribution becomes dominant, only small deformations were considered in the numerical model. Consequently, the computed deformations are slightly lower than the experimental values.

3.4 Lattice truss beam with reinforced concrete frame ( Santarella, Luigui [25]). )

A lattice truss structure with upper and lower frames has a theoretical clear span of 12 m, and a height of 2 m between the axes of the members. Construction details are shown in Figure 11. The dimensions were chosen so that, under self-weight or under any of the following loading conditions, the compressive stress in the concrete does not exceed 30 kg/cm², and the steel bars remain in tension.

The loading conditions are as follows:

1. Concentrated load of 39 kN at each upper node;
2. Concentrated load of 39 kN at each lower node;
3. Uniformly distributed load of 2 kN per linear metre along the upper nodes;

Uniformly distributed load of 2 kN per linear metre along the lower nodes.

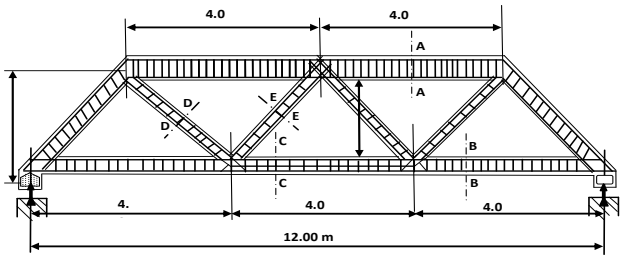


Figure 11. Construction details of the lattice truss structure with upper and lower frames

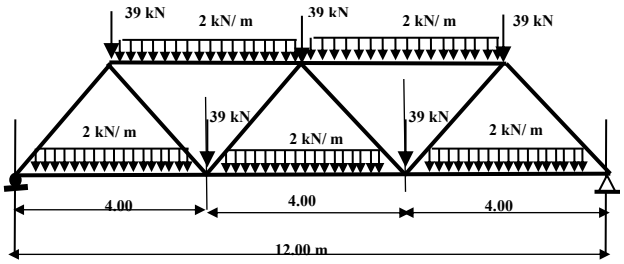


Figure 12. The loading of the lattice truss structure

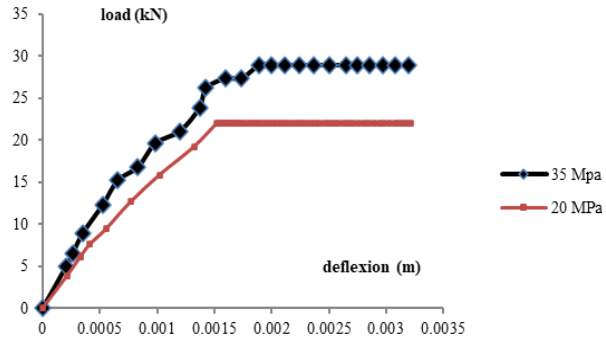


Figure 13. Load-displacement relation

The analysis was carried out for concrete compressive strengths of 20 and 35 MPa. A numerical study of the elastic behavior of the lattice truss structure shown in Figure 5 indicates that, for a compressive strength of 20 MPa, a 39 kN load does not lead to failure and the structural response remains elastic. For a compressive strength of 35 MPa, however, the numerical results show nonlinear behavior. According to Santarella and Luigi, the structure remains perfectly elastic for a concrete compressive strength of 30 MPa.

## 4. Conclusion

In our study, a numerical model was developed to simulate the nonlinear behavior of prestressed concrete beams and reinforced concrete trusses. The results show that the method is reliable and can accurately predict cracking, material degradation, and the effect of fibers. Some limitations remain, such as the model not including long-term effects like creep and shrinkage. Future work will extend the model to larger structures and explore different fiber configurations to improve performance.

$\boldsymbol{E_{b0}}$ ; $\boldsymbol{\varepsilon}$ ; $\boldsymbol{f_{cj}}$ ; $\boldsymbol{f_{tj}}$ ; $\boldsymbol{\varepsilon_{b0}}$ as show in figure 1
$\boldsymbol{E_{ct}}$ Initial modulus of the composite in tension
$\boldsymbol{f_{ft}}$ $\boldsymbol{\varepsilon_u}$ as show in figure 2
$\boldsymbol{\varepsilon_r}$ Fracture strain of the composite
$\boldsymbol{\sigma_{uc}}$ Residual stress: $\boldsymbol{\sigma_{uc} = \bar{\omega}\theta_o\, l_f\, \tau_u/\phi}$
$\bar{\boldsymbol{\omega}}$ Percentage of fibers
$\boldsymbol{\theta_o}$ Fiber orientation coefficient
$\boldsymbol{l_f}$ Length of the fiber
$\boldsymbol{\tau_u}$ Ultimate bounding stress of the fiber
$\boldsymbol{\phi}$ Diameter of the fiber
$\boldsymbol{k_b}$ and $\boldsymbol{k_b'}$ Dimensionless parameters of the Sargin low
$[\boldsymbol{K}]$ Stiffness matrix
$\{\Delta\boldsymbol{U}\}$Vector of nodes displacements increase
$\{\Delta\boldsymbol{F}\}$ Vector nodes forces increase
$\{\Delta\boldsymbol{P}\}$ Vector of applied loads increas

## 5.List of nomenclaturteres

## 6.References


[1] Bouafia, Y., Kachi, M. S., & Fouré, B. (2002). Relation contrainte-déformation en traction du béton armé de fibres d'acier. Annales du Bâtiment et des Travaux Publics.

[2] Felippa, C. A. (2001). Nonlinear finite element methods. University of Colorado Boulder. (Available at http://www.colorado.edu/engineering/CAS/courses.d/NFEM.d/Home.html )

[3] Albermani, F., Mahendran, M., & Kitipornchai, S. (2004). Upgrading of transmission towers using a diaphragm bracing system. Engineering Structures, 26 (6), 735–744. https://doi.org/10.1016/j.engstruct.2004.01.004

[4] Bouafia, Y. (1991). Résistance à l'effort tranchant des poutres en béton à précontrainte extérieure : étude expérimentale et calcul à la rupture [Thèse de doctorat, École Centrale des Arts et Manufactures, Paris].

[5] Iguetoulene, F., Bouafia, Y., & Kachi, M. S. (2017). Non-linear modeling of three-dimensional reinforced and fiber concrete structures. Frontiers of Structural and Civil Engineering, 11 (3), 293–307. https://doi.org/10.1007/s11709-017-0418-6

[6] Bouafia, Y., Kachi, M. S., & Fouré, B. (1998). Relation contrainte-déformation dans le cas du béton armé de fibres d'acier. Annales du Bâtiment et des Travaux Publics, (2), 5–17.

[7] Grelat, A. (1978). Analyse non linéaire des ossatures hyperstatiques en béton armé [Thèse de docteur-ingénieur, Université Paris VI].

[8] Bazeos, N., & Xykis, C. (2002). Elastic buckling analysis of 3-D trusses and frames with thin-walled members. Computational Mechanics, 29 (6), 459–470. https://doi.org/10.1007/s00466-002-0355-6

[9] Nait-Rabah. (1990). Simulation numérique des ossatures spatiales [Thèse de doctorat, École Centrale de Paris].

[10] Park, S. H., Kim, D. J., Ryu, G. S., & Koh, K. T. (2012). Tensile behavior of ultra high performance hybrid fiber reinforced concrete. Cement and Concrete Composites, 34 (2), 172–184. https://doi.org/10.1016/j.cemconcomp.2011.09.009

[11] Règles B.A.E.L. 91 modifiées 99. (2000). Règles techniques de conception et de calcul des ouvrages et constructions en béton armé suivant la méthode des états limites. Eyrolles.

[12] Riks, E. (1972). The application of Newton's method to the problem of elastic stability. Journal of Applied Mechanics, 39 (4), 1060–1066. https://doi.org/10.1115/1.3422829

[13] Zhan. (1991). Contribution au dimensionnement des pieux en béton de fibres [Thèse de docteur, Laboratoire C.E.B.T.P.].

[14] Iguetoulene, F., Bouafia, Y., & Kachi, M. S. (2024). Incremental analysis for the nonlinear buckling responses of the reinforced concrete and the steel spatial arch truss structure subjected to displacement dependent loads. International Journal of Structural and Civil Engineering Research, 13 (1), 1–9. (Article in press; DOI may be assigned later.)

[15] Bouafia, Y., Kachi, M. S., & Fouré, B. (2000). Numerical modeling of the behavior of steel fiber reinforced concrete. Proceedings of the II International Conference on Cement and Concrete.

[16] Bouafia, Y., & Adjrad, A. (1997). Utilisation des fibres locales pour renforcement du béton. Séminaire National de Génie Civil, M'sila (Algérie).

[17] Adjrad, A., Kachi, M. S., Bouafia, Y., & Iguetoulene, F. (n.d.). Nonlinear modeling of structures in 3D. Proceedings of the 4th Annual ICSAAM, 1–9.

[18] Benyahi, K., Bouafia, Y., Barboura, S., & Kachi, M. S. (2018). Nonlinear analysis and reliability of metallic truss structures. Frontiers of Structural and Civil Engineering, 12 (4), 577–593. https://doi.org/10.1007/s11709-018-0487-0

[19] Bouchafa, D., Kachi, M. S., Bouafia, Y., Benyahi, K., & Barboura, S. (2021). Numerical simulation and reliability of behaviour until the rupture of reinforced concrete spatial structure members with circular cross section. Journal of Materials and Engineering Structures, 8 (1), 61–82. (May be obtained at http://revue.ummto.dz/index.php/JMES/article/view/2471 )

[20] Jamshidi, M. (2023). The effect of polypropylene fibers on the behavior of fiber self-compacting concrete. Journal of Rehabilitation in Civil Engineering, 11 (2), 85–98. https://doi.org/10.22075/jrce.2022.26076.1582

[21] Parvinnejad, A., Amiri, M., & Dabbagh, H. (2022). Effect of steel and hybrid fibers on the impact resistance of concrete with FRP sheets. Structures, 45 , 163–176. https://doi.org/10.1016/j.istruc.2022.09.004

[22] Kameli, S., Shahi, S., & Mahboob, S. (2024). Investigating mechanical properties of natural fiber-reinforced concrete. Innovative Infrastructure Solutions, 9 , 141. https://doi.org/10.1007/s41062-024-01489-9

[23] Zedan, H. H., & Khan, M. (2023). Modelling fibre reinforced concrete for predicting optimal mechanical properties. Journal

of Engineering and Applied Science, 70 , 35. https://doi.org/10.1186/s44147-023-00207-5

[24] Al-Mahaidi, R., & Kalfat, R. (2022). Finite element modelling of reinforced concrete beams strengthened with FRP composites. Composite Structures, 300 , 116158. https://doi.org/10.1016/j.compstruct.2022.116158

[25] Santarella, L. (1919). Efforts secondaires dans les travées à treillis en béton armé. Schweizerische Bauzeitung, 73 (19), 221–223. https://doi.org/10.5169/seals-3409